HAL
open science

Competition of elastic and adhesive properties of carbon nanotubes anchored to atomic force microscopy tips

Charlotte Bernard, Sophie Marsaudon, Rodolphe Boisgard, Jean-Pierre Aimé

To cite this version:

Charlotte Bernard, Sophie Marsaudon, Rodolphe Boisgard, Jean-Pierre Aimé. Competition of elastic and adhesive properties of carbon nanotubes anchored to atomic force microscopy tips. Nanotechnology, 2008, 19 (3), pp.035709 (1-10). 10.1088/0957-4484/19/03/035709 . hal-00250904

HAL Id: hal-00250904

https://hal.science/hal-00250904v1

Submitted on 12 Feb 2008

HAL is a multi-disciplinary open access archive for the deposit and dissemination of scientific research documents, whether they are published or not. The documents may come from teaching and research institutions in France or abroad, or from public or private research centers.

L'archive ouverte pluridisciplinaire **HAL**, est destinée au dépôt et à la diffusion de documents scientifiques de niveau recherche, publiés ou non, émanant des établissements d'enseignement et de recherche français ou étrangers, des laboratoires publics ou privés.

Competition of Elastic and Adhesive Properties of Carbon Nanotubes Anchored to Atomic Force Microscopy Tips.

Charlotte Bernard, Sophie Marsaudon*, Rodolphe Boisgard, Jean-Pierre Aimé

s.marsaudon@cpmoh.u-bordeaux.fr

Université Bordeaux 1- CPMOH 351 cours de la Libération , 33405 Talence cedex France

Abstract

In this paper we address the mechanical properties of carbon nanotubes anchored to atomic force microscopy (AFM) tips in a detailed analysis of experimental results and exhaustive description of a simple model. We show that volume elastic and surface adhesive forces both contribute to the dynamical AFM experimental signals. Their respective weight depends on the nanotube properties and on an experimental parameter : the oscillation amplitude. To quantify the elastic and adhesive contributions, a simple analytical model is used. It enables analytical expressions of the resonance frequency shift and dissipation that can be measured in atomic force microscopy dynamical frequency modulation mode. It includes the nanotube adhesive contribution to the frequency shift. Experimental data for single-wall and multi-wall carbon nanotubes compare well to the model predictions for different oscillation amplitudes. Three parameters can be extracted : the distance necessary to unstick the nanotube from the surface and two spring constants corresponding to tube compression and to elastic force required to overcome the adhesion force.

1 Introduction

Since their discovery [1], carbon nanotubes (CNT) have attracted many scientists attention. Unique electronic properties have been demonstrated for their use in molecular electronics and integrated electronic devices [2]. Many CNT applications now turn to use their excellent mechanical properties as nanoswitches [3](for binary memory device), motors [4], actuators [5, 6] or material reinforcement [7]. As expected for one of the strongest bond as the C-C covalent in plane graphite bond, CNT have a high Young modulus, up to 1 TPa (10^{12} P, as compared to diamond value 1.2 TPa) [8, 9, 6, 10] and they can endure severe structural distortion up to the ability to buckle elastically. Besides those excellent properties, inserting CNT into MEMS or NEMS may face new difficulties as the control of their anchoring to the structure, or else the loss of mechanical properties [11]. As an example, the excellent mechanical properties of CNT may be lost if the nanotubes are not properly anchored to the moving device. In this paper, we investigate the mechanical properties of CNT anchored to atomic force microscopy (AFM) probes. In this context, the mechanical behavior of the CNT is the result of a competition between volume forces, the elastic contribution, and surface forces, the adhesive

contribution.Only two forces are considered to describe the tube interaction with surfaces, an elastic repulsive one as the nanotube bends over the surface and an attractive adhesive one, giving analytical expressions for the dynamical AFM signals. The model expressions are compared to many experimental signals for multi-wall and single-wall CNT.

2 Experiment

The single-wall (or double-wall here after called single-wall for clarity) CNT probes are fabricated directly on commercial silicon tips by hot filament chemical vapor deposition, whereas the multi-wall CNT are grown on a filament and then welded to commercial silicon tips for atomic force microscopy (AFM), following procedures already published [12, 13]. The cantilever/tip oscillators are NCL from Nanosensors, they have resonance frequency in the range of 150-200 kHz, cantilever stiffness of 10 to $50N.m^{-1}$, quality factors Q of about 500 in air and 2000 at 8mbar when very far from the surface (some microns at least). They have been selected for their well defined harmonic behavior. An example of a multi-wall CNT anchored on a commercial pyramidal tip is given in figure 1.

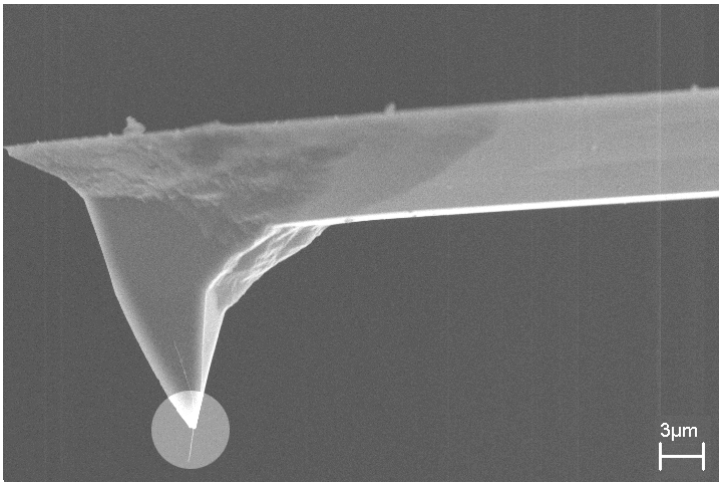

Figure 1: Scanning electron microscopy image of a tip/cantilever on which an multi-wall CNT has been welded at the tip apex (lighter circle).

The mechanical behavior of the CNT probes is recorded during approach toward a surface (freshly cleaved highly oriented graphite or silica) in atomic force microscopy experiments in dynamical frequency modulation mode. In this mode, an electronic feedback loop maintains the oscillator phase shift to the resonance value ($-\pi/2$). The resonance frequency shift due to interaction is recorded. This frequency shift is due to force gradient. To maintain the oscillation amplitude at a fixed value, another loop is used; its error signal, called Damping (expressed in Volts) is recorded. It is proportional to the energy needed to keep the oscillation amplitude constant. This dynamical mode enables non ambiguous separation of conservative forces (in the frequency signal) and dissipative forces (in Damping signal). The experiments are carried on a modified contact Veeco head, with a Nanoscope III controller and Nanosurf PLL electronics. The curves are recorded under vacuum (around 8 mbar) to reduce the surface contamination and to increase the quality factor, thus increasing the energy sensitivity of the experiment.

To compare the experimental data to the model, the frequency shifts are normalized with the resonance frequency without interaction with the surface, the piezo ceramic displacement is

transformed to nanotube-surface displacement by setting the onset of frequency shift variation at a distance D=A (A being the oscillation amplitude), see figure 2.

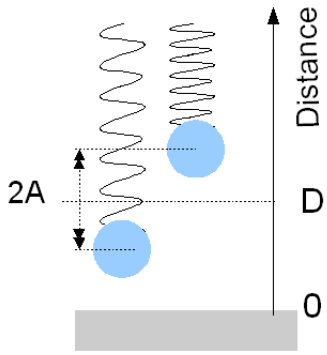

Figure 2: Scheme of the equivalent oscillator in the two extremal positions when oscillating at an amplitude A. D is the distance between the oscillator equilibrium position and the surface.

The dissipated energy per oscillation cycle is $E = \pi\gamma\omega A^2$, with $\omega = 2\pi\nu$ the oscillator pulsation and ν its frequency. When the tip touches the surface, a simple sum rule is usually applied to describe the total dissipated energy:

$$E_{tot} = E_0 + E_{int}$$

with E_{tot} the total mean dissipated energy, E_0 the mean dissipated energy without interaction with the surface and E_{int} the energy dissipated due to the contact between the CNT and the surface. The corresponding damping coefficient γ_{tot} writes:

$$\gamma_{tot} = \gamma_0 + \gamma_{int}$$

with $\gamma_0 = \frac{k_c}{\omega Q}$ the damping of the oscillator without interaction (k_c is the cantilever stiffness) and γ_{int} the damping coefficient due to interaction.

The proportionality between the Damping signal and damping coefficient gives:

$$\frac{Damp_{tot}}{Damp_0} = \frac{\gamma_{tot}}{\gamma_0} = \frac{E_{tot}}{E_0}$$

and thus :

$$\begin{aligned} \gamma_{int} &= \left(\frac{Damp_{tot}}{Damp_0} - 1\right)\gamma_0 \\ E_{int} &= \left(\frac{Damp_{tot}}{Damp_0} - 1\right)E_0 \end{aligned} \tag{1}$$

Equation 1 will be used to derive the mean energy dissipated from the Damping signal and experimental parameters.

3 Material and Method

The description of the mechanical behavior of the CNT squeezed between the tip apex and the surface is based on two main assumptions :

- the cantilever spring constant is much larger than the CNT one;

-the contact stiffness, governed by the contact area between the CNT free end and the surface, is also much larger than the CNT bending stiffness.

In these experiments, the typical CNT bending stiffness of SWNT and MWNT vary between 10^{-4} and a few $10^{-2} Nm^{-1}$. Therefore, the first constraint is always easily satisfied, as the cantilever spring constant is larger than $10\,Nm^{-1}$. The contact stiffness between a tip and a surface scales with the reduced Young modulus [14] that here we note G and with the the diameter of the contact area between the tip and the surface ϕ. Even with a soft material and a very small contact area, for instance a polystyrene substrate with $G = 1$GPa and a contact diameter of $1\,nm$, the contact stiffness reaches a value of $1\,N.m^{-1}$ that remains very large compared to the CNT bending one. However, as shown below, to pull off the CNT from the surface it is necessary to consider another CNT spring constant related to the extension of the CNT rather than the bending stiffness. Typical values of this pull off spring constant vary between 0.05 and $0.1\,Nm^{-1}$thus are also much smaller than any reasonable values of the contact stiffness. Therefore, the experimental measurements only contain information on the mechanical properties of the CNT squeezed between the cantilever and the surface, including the elastic response and the adhesion between the part of the tube touching the surface.

To introduce the model we proceed in two steps. First, a general approach in which the forces acting on the oscillator are decomposed into Fourier coefficients : this part may be applied for many different systems. Somehow, the derivation is similar to the one employed by U. Dürig [15]. Then, we focus on the specific CNT case, and two spring constants are introduced, one to account for the repulsive elastic response of the bending nanotube, the second to account for the pull off force required to unstick the nanotube from the surface.

3.1 Least action principle and Fourier analysis of the force

To take into account the interaction between the tip and the surface, the interaction Lagrangian L_i is added to the Lagrangian of the harmonic oscillator [16]:

$$L = \frac{1}{2}m\dot{Z}^2 - \frac{1}{2}m\omega_0^2 Z^2 + FZ\cos\omega t - \gamma_0 Z\underline{\dot{Z}} + L_i$$

where Z is the oscillator instantaneous displacement with the equilibrium position, m its effective mass, F the intensity of the force acting on it, and L_i the interaction Lagrangian with the force calculated along the physical path $\underline{Z}$:

$$L_i = F_i\left(\underline{Z}\right) Z$$

To include dissipation process into the Lagrangian description [17], the underscored variables are not varied during the minimization [16, 18].

We then consider an harmonic solution , $Z\left(t\right) = A\cos\left(\omega t + \phi\right)$, and apply the least action principle to get :

$$\left\{ \begin{array}{c} m\omega_0^2\left(\frac{\omega^2}{\omega_0^2} - 1\right)A = -\frac{2}{T}\int_0^T F_i\left(Z\right)\ \cos\left(\omega t + \phi\right)\ dt \\ F = \gamma_0 A\omega + \frac{2}{T}\int_0^T F_i\left(Z\right)\ \sin\left(\omega t + \phi\right)\ dt \end{array} \right. \tag{2}$$

Let's define the Fourier coefficients for the interaction force in the phase space : $\theta = \omega t$, and a time origin when the elongation is at its maximal value

$$\begin{cases} f_i = \frac{1}{\pi} \int_{-\pi}^{\pi} F_i(\theta) \ \cos(\theta) \ d\theta \\ g_i = \frac{1}{\pi} \int_{-\pi}^{\pi} F_i(\theta) \ \sin(\theta) \ d\theta \end{cases} \tag{3}$$

Using the approximation for a pulsation close to its resonance free value $\frac{\omega^2}{\omega_0^2} - 1 \simeq 2\frac{\Delta\omega}{\omega_0}$ and $F = \gamma\omega A$ in equation 2 gives:

$$\begin{cases} \frac{\Delta\omega}{\omega_0} = -\frac{1}{2kA} f_i \\ \gamma = \gamma_0 + \gamma_i \end{cases} \tag{4}$$

with

$$\gamma_i = \frac{1}{A\omega_0} g_i$$

3.2 Application to the carbon nanotubes interacting with the surface : resonance frequency shift and dissipation

A simple model has been built, based on continuum mechanical model of a beam pinned at one end approaching toward a surface and bending while gliding over it. The experiment may lead to rather complicate relationships between the force and nanotube displacement in both attractive and repulsive regime. However, let assume a linear relationship between force and position for repulsive and attractive interaction, corresponding to compression (in repulsive regime) and elongation (in attractive regime) of the CNT interacting with the surface, as depicted in figure 3. The slope of the force curves defines two nanotube stiffness : an equivalent repulsive one k_{r} for the elastic repulsive force and an equivalent attractive one for the extension part.Therefore, other parameters that may be relevant will not be considered here, for instance, the influence of the nanotube angle as respect to the surface as developed by other authors [19, 20, 21] or else change of the contact area as a function of the vertical displacement.

The presence of an adhesive interaction breaks the time reversal as schemed by the arrows of figure 3 and induces dissipation as described in reference [15]. As the system stiffness is not infinite, adhesion hysteresis occurs that is governed by the softer element, in the present experiment the carbon nanotube [22]. This kind of cycle with mechanical elements of finite stiffness is known also in other areas, as for instance the adsorption-desorption of atoms on surface leading to similar dissipation. The shadowed area shown in figure 3 gives the adhesion hysteresis of the nanotube on the surface.

Using those equivalent stiffness with a force threshold necessary to unstick will enable to get final analytical relationships between the oscillator resonance frequency shift and the nanotube movement.

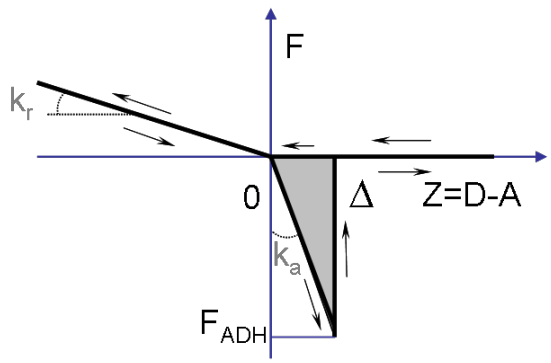

Figure 3: Scheme of the forces acting on the nanotube against CNT displacement when interacting with the surface : during the approach, only elastic repulsion when the nanotube touches the surface (elastic spring constant k_r); and during the retract elastic repulsion then an attractive force to unstick from the surface during the distance $\triangle$ until it reaches the force threshold F_{adh} (spring constant k_a).

3.2.1 Vertical forces acting on the nanotube in intermittent contact

- Forces expressions

Following figure 3, the time or equivalently the phase limits for the two forces are set :

$$F_i(\theta) = \begin{cases} -k_r(A\cos(\theta) - D) \;\; for \; -\theta_r \leq \theta \leq \theta_r \\ -k_a(A\cos(\theta) - D) \;\; for \, \theta_r \leq \theta \leq \theta_\Delta \end{cases} \tag{5}$$

where the phases θ_r and θ_Δ are linked to the duration of the compression and extension phase respectively of the nanotube :

$$\begin{cases} \theta_r = \arccos(d) \\ \theta_\Delta = \arccos(d - \delta) \end{cases}$$

A plot of the force variation within one oscillation period in intermittent contact is given in figure 4. Far from the surface, on the left side of the curve, the force on the CNT is null up to the first touch with the surface which happens at $-\theta_\mathrm{r}$, then the CNT is compressed. On the way back from the surface (corresponding to $\omega t > 0$), the CNT is compressed again up to θ_r, then it is extended up to the time θ_Δ.

- Relative frequency shift due to repulsive interactions

According to equations 3 , 4 and 5 , the relative pulsation shift $\Delta\omega_\mathrm{r}$ due to the elastic repulsive force is :

$$\frac{\Delta\omega_r}{\omega_0} = \frac{1}{2\pi k_c}\left\{k_r\left(\arccos(d) - d\sqrt{1-d^2}\right)\right\} \tag{6}$$

This expression is identical to the one obtained without using development in Fourier coefficients [23, 24]. Figure 5a shows the variation of the relative repulsive frequency shift as a function of the normalized distance for two CNT bending stiffness k_r. As expected, when the CNT moves towards the surface (corresponding to decreasing d), its interaction time with the surface increases leading to increasing frequency shift.

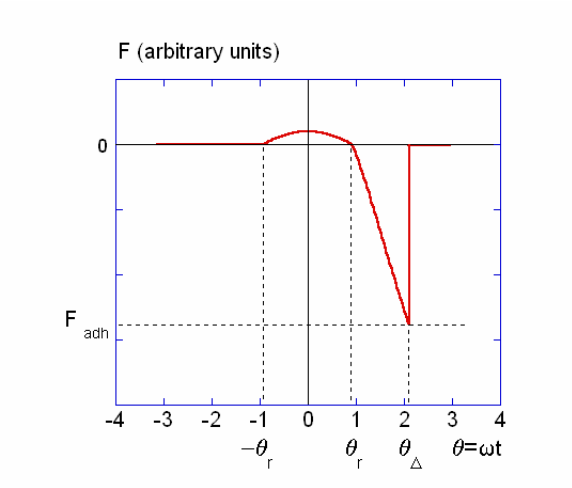

Figure 4: Variation of the force acting on the CNT with the phase variable $\theta = \omega t$ during one oscillation period for intermittent contact. Stiffness values are $k_{\mathrm{r}} = 0.0001\, N.m^{-1}$ and $k_{\mathrm{a}} = 0.001\, N.m^{-1}$.

- Relative frequency shift due to attractive interactions

The same calculation can be done to predict the contribution of the attractive force on the relative pulsation shift $\Delta\omega_{\mathrm{a_i}}$:

$$\frac{\Delta\omega_{\mathrm{a_i}}}{\omega_0} = \frac{1}{2\pi k_c}\left\{\frac{k_a}{2}\left(\arccos\left(d-\delta\right) - \arccos\left(d\right) + d\sqrt{1-d^2} - \left(d+\delta\right)\sqrt{1-\left(d-\delta\right)^2}\right)\right\} \quad (7)$$

where δ is the normalized distance necessary to unstick from the sample : $\delta = \frac{\Delta}{A}$.

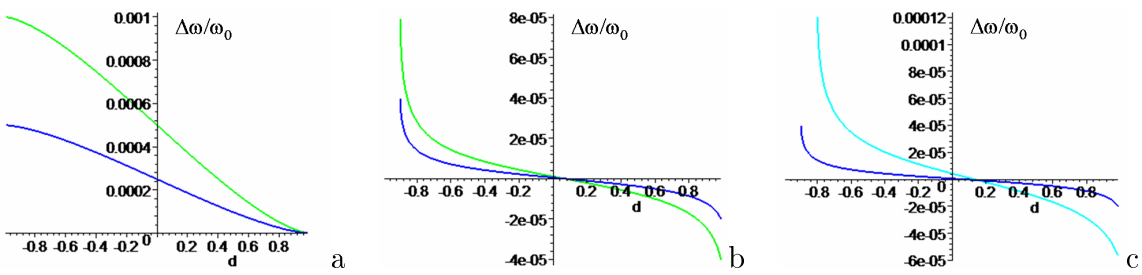

Figure 5: Relative frequency shift variation with normalized distance d. Fig.a : relative frequency shift for elastic repulsive interaction (according equation 6) for two CNT stiffness values : $0.001k_c$ and $0.002k_C$. Fig.b : relative frequency shift variation (expression 7) for attractive adhesive interaction with equivalent adhesive stiffness of $0.01k_c$ and $0.02k_c$. Fig.c : relative frequency shift variation (expression 7) with normalized distance for attractive adhesive interaction with an equivalent adhesive stiffness of $0.01k_c$ and two normalized sticking distances $\delta = \frac{\Delta}{A}$: $0.1A$ and $0.2A$.

Results derived from equation 7 are plotted in Fig. 5b for two attractive stiffness values k_a and one value of δ, and in Fig. 5c for one equivalent attractive stiffness value and two values of δ. The attractive force contributes to the pulsation shift mainly at the beginning and at the end of the intermittent contact domain, with shift values one order of magnitude lower than the repulsive ones of Fig. 5a, despite the factor ten between the attractive and repulsive stiffness values. The smaller contribution of adhesive force to the frequency shift as compared

to the elastic bending force is due to the limited interaction time τ_Δ of the attractive force as compared to the constantly increasing interaction time of the elastic force. Increasing the normalized sticking distance δ value increases the attractive contribution as expected for longer interaction time τ_Δ, but also shrinks the size of the intermittent contact domain given by $2A - \Delta$. Note that, when the elastic spring constant of the NT is large $\triangle$ may be small and the adhesive contribution to the frequency shift becomes negligible leading to an intermittent contact size of $2A$ [23] .

- Dissipation

As said above, the mechanical cycle leads to a dissipated energy given by the triangular shadowed area in Fig.3:

$$E_{adh} = \frac{1}{2} k_a \Delta^2 \tag{8}$$

It is thus constant all over the intermittent contact domain and does not depend on the oscillation amplitude A.

3.2.2 Vertical forces acting on the nanotube in permanent contact

- Forces expressions due to the attractive and repulsive interactions

Compared to the set of equations 5, the difference is the time during which the equivalent attractive spring constant acts over the oscillation period:

$$F_i(\theta) = \begin{cases} -k_r\left(A\cos(\theta) - D\right) \;\; for \; -\theta_r \leq \theta \leq \theta_r \\ -k_a\left(A\cos(\theta) - D\right) \;\; for \; -\pi \leq \theta \leq \theta_r \; and \; \theta_r \leq \theta \leq \pi \end{cases} \tag{9}$$

In opposition to the intermittent contact case, the attractive force is now exerted twice on the CNT within an oscillation period as depicted in Fig.6.

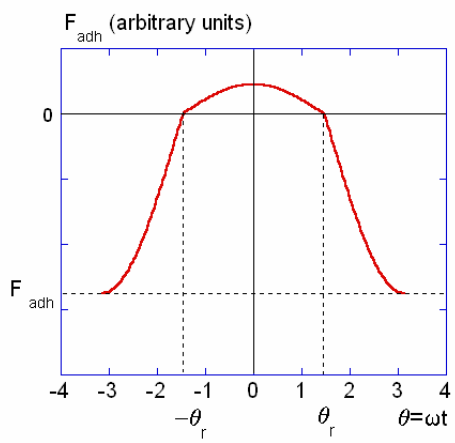

Figure 6: Variation of the force acting on the CNT with the phase variable $\theta = \omega t$ during one period for permanent contact

- Relative frequency shift due to the attractive contribution

No change happens for the repulsive force, the expression of the repulsive frequency shift is thus the same as the one given in the equation 6. On the contrary, the attractive contribution increases as soon as the CNT does not unstick from the surface with an instantaneously doubling of the attractive force during the oscillation cycle Fig.6. The relative frequency shift$\Delta\omega_{\mathrm{a_p}}$ becomes :

$$\frac{\Delta\omega_{\mathrm{a_p}}}{\omega_0} = \frac{1}{2\pi k_c}\left\{k_a\left(\pi - \arccos(d) + d\sqrt{1-d^2}\right)\right\} \tag{10}$$

The result given by the equation 10 (permanent contact) can be readily compared to the one given by the equation equation 7 (intermittent contact) by setting $\delta = d$. One gets the result :

$$\left.\frac{\Delta\omega_{\mathrm{a_i}}}{\omega_0}\right|_{d=\delta} = \frac{1}{2}\left.\frac{\Delta\omega_{\mathrm{a_p}}}{\omega_0}\right|_{d=\delta} \tag{11}$$

Equality 11 shows that the frequency shift must jump to a higher value at the transition from the intermittent contact to the permanent one.

The jump can be understood with the help of the plot shown in figure 6: the supplementary attractive force in permanent contact has a phase shift of π as respect to the initial intermittent contact one of figure 4. This phase lag inverses the attractive contribution to the frequency shift. A similar conclusion had been found earlier [25] for an attractive van der Waals force on a vibrating tip.

- Dissipation

As soon as the nanotube becomes unable to pull off the surface, the asymmetry in force in each oscillation cycle vanishes, and no additional energy will be dissipated.

3.2.3 Summary - table

Table 1 presents the final pulsation shift and dissipation expressions in the intermittent and permanent contact of the CNT with the surface. Those expressions are obtained by adding the repulsive and attractive contributions.

type of contact	relative frequency shift	dissipation
intermittent	$\frac{\Delta\omega}{\omega_0} = \frac{1}{2\pi k_c}\left\{\begin{array}{c} k_r\left(\arccos(d) - d\sqrt{1-d^2}\right) \\ +\frac{k_a}{2}\left(\arccos(d-\delta) - \arccos(d) + d\sqrt{1-d^2} - (d+\delta)\sqrt{1-(d-\delta)^2}\right)\end{array}\right\}$	$E_{int} = \frac{1}{2}k_a\Delta^2$
permanent	$\frac{\Delta\omega}{\omega_0} = \frac{1}{2\pi k_c}\left\{k_r\left(\arccos(d) - d\sqrt{1-d^2}\right) + k_a\left(\pi - \arccos(d) + d\sqrt{1-d^2}\right)\right\}$	$E_{int} = 0$

Table 1: Final expressions of the pulsation shifts and dissipation obtained from the model including the elastic bending force and the pull off force.

Figure 7 presents the theoretical curves calculated from the expressions given in the table 1. The three regime domains are highlighted :

1. no interaction for $d > 1$: no frequency shift , no added dissipation
2. intermittent contact regime for $-0.8 < d < 1$: first negative frequency shift due to main attractive force then increasing repulsive contribution ; contact dissipated energy due to adhesion hysteresis.
3. permanent contact regime for $d < -0.8$: decreasing frequency and no additional energy dissipated.

Note the frequency jump and vanishing of the dissipated energy happen at the same vertical location.

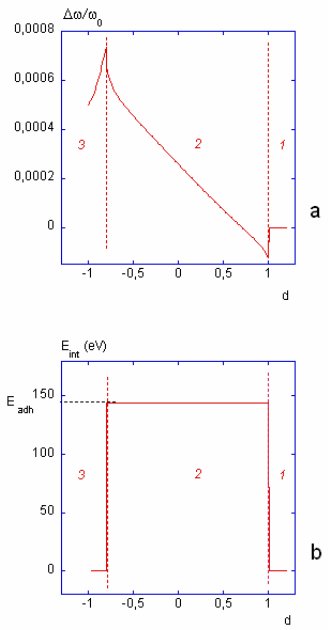

Figure 7: Theoretical variation of relative frequency shift and dissipation obtained from the model. The parameters values are $\frac{k_r}{k_c} = 0.0001$, $\frac{k_a}{k_c} = 0.001$ and $\delta = 0.2$ for the normalized pulsation. To obtain the energy dissipated value, the cantilever stiffness is $30\,N.m^{-1}$ and the oscillation amplitude is $200\,nm$.

The attractive force with the distance necessary to unstick Δ reduces the size of the intermittent contact domain from $2A$ (as reported previously [23] when non attractive force was considered) to $2A - \Delta$.

3.3 Amplitude influence

In contrary to the pure elastic case [23], the presence of the normalized distance δ in the attractive parts (table 1) predicts change in the frequency shift as a function of the oscillation amplitude (figure 8). Varying the oscillation amplitude corresponds to change of the adhesive interaction time within the oscillation cycle : the smaller the amplitude, the larger the adhesive interaction time in the oscillation period. Thus the balance between the volume elastic repulsive force and the surface adhesive force can be experimentally finely tuned by changing the oscillation amplitude.

As shown in figure 8, when δ increases (corresponding to small amplitudes), the elastic bending contribution on the frequency shift can disappear up to the point where only the frequency jump remains.

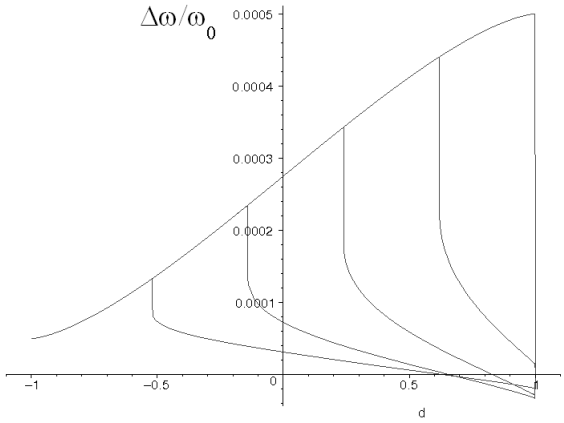

Figure 8: Plot of the theoretical relative pulsation shift against the normalized distance d for different values of δ. The parameter values are : $k_r/k_c = 0.0001; k_a/k_c = 0.001$; and $\delta = 0.1$; 0.49; 0.87; 1.35; 1.73. Changing $\delta = \frac{\Delta}{A}$ value can be done experimentally by changing the oscillation amplitude for one given CNT.

4 Results and Discussion

4.1 Results obtained on multi-wall CNT

4.1.1 Experimental results

Figures 9b and c present experimental relative frequency shifts $\frac{\Delta\nu}{\nu_0}$ and energy dissipated E_{int} collected with the multi-wall CNT shown in figure 9a .

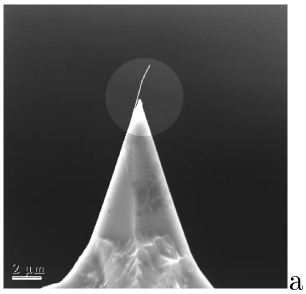

a

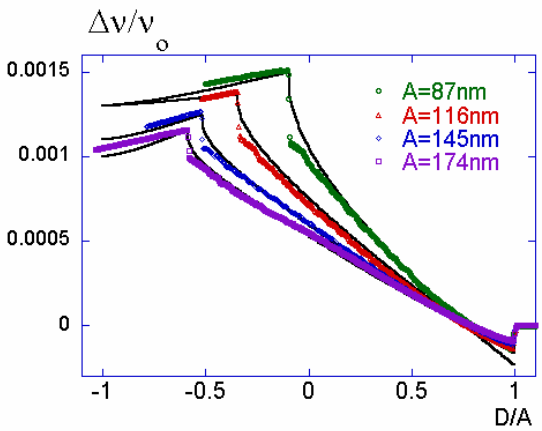

b

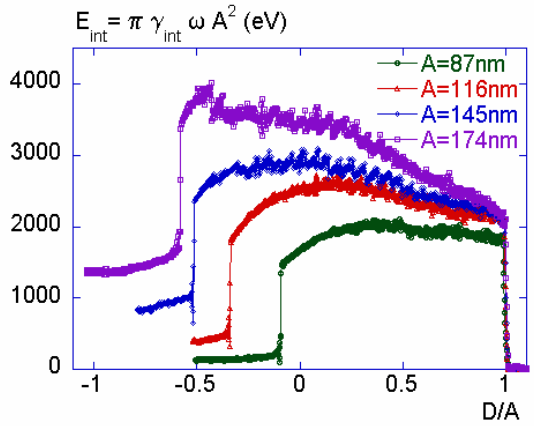

c

Figure 9: multi-wall CNT data. Figure 9.a : Scanning electron micrograph of the multi-wall used. Its estimated length L and radius r are $3.5\mu m$ and $30nm$ respectively. Figure 9b : Experimental relative frequency shift (color dots) compared to model expressions (black solid lines) for four oscillation amplitudes. Figure 9c: corresponding interaction energy dissipated.

The three regimes predicted by the model are clearly identified both in the frequency shifts and dissipated energies. From the right to the left :

1. no interaction : first the CNT does not interact with the surface, the resonance frequency is the oscillator free one, the frequency shift is null and no additional dissipation occurs.

2. intermittent contact: the frequency first decreases due to the attractive interaction then increases as the bending of the NT increases. The dissipated energy varies only slightly during the intermittent regime and exhibits a weak dependence on the oscillation amplitude.

3. permanent contact: the transition between the two regimes is marked by the rapid frequency increase and, simultaneously, by a vanishing dissipated energy.

Note also that the size of the intermittent regime domain reduces as the oscillation amplitude decreases.

4.1.2 Frequency shifts

The frequency shifts displayed in figure 9b are fitted with the expressions given in table 1. For the four amplitudes, the calculated values are in good agreement with the overall experimental frequency variations . The parameters are the normalized stiffness k_r/k_c and k_a/k_c as the distance Δ is an experimental value given by the location of the frequency jump at the transition between the intermittent and permanent regime : $\Delta \approx 75\,nm$.

The normalized equivalent stiffness values for the different amplitudes are $\frac{k_r}{k_c} \approx 0.0015$ and $\frac{k_a}{k_c} \approx 0.003$.Those stiffness ratio are coherent with the assumption that the nanotube should display the softest stiffness as compared to the cantilever and the contact stiffness. Assuming a value of the cantilever stiffness of $30N.m^{-1}$ gives a bending stiffness of $k_\mathrm{r} \approx 0.04\,N.m^{-1}$ and $k_\mathrm{a} \approx 0.1\,N.m^{-1}$. The k_r value is of the same order of magnitude than the CNT bending stiffness assuming the CNT to be a cylinder : $k_\mathrm{b} = \pi E \frac{r^4}{L^3} \approx 0.08\,N.m^{-1}$. The pull off force can be evaluated : $F_{adh} = k_{adh}\Delta \approx 7.5\,nN$. This value can be compared to values obtained with other studies. Walkeajärvi et al [26] calculated an adhesive force between multi-wall CNT with smaller radius (3-13 nm) and lithographically fabricated gold lines of 0.2 to $2.3\,nN$, values similar but slightly inferior than the one obtained here.

Assuming a nanotube gliding along the graphite surface, we can consider the adhesion force of a tube on a surface [27] : $F_{adh} = \frac{H\sqrt{r}}{12\sqrt{2}d_c^{5/2}}L_c$ with $d_c = 0.165\,nm$ the smallest distance between the nanotube and the surface, $H = 5.10^{-20}\,J$ the Hamaker constant and $L_c$the contact length between the nanotube and the plane surface. The value of F_{adh} gives a contact length of about $6\,nm$.

4.1.3 Dissipation

From k_{adh} and Δ values given by the frequency shifts, the dissipated energy due to the mechanical hysteresis can also be evaluated : $E_{dissipated} = \frac{1}{2}k_{adh}\Delta^2 \approx 1710\,eV$. This value has to be compared to the experimental interaction energy. Disregarding other processes as influence of the friction force, we concentrate on the height of the first energy jump at $d = \frac{D}{A} = 1$. This height is : $E_{int} \approx 1790 - 2090\,eV$, again an experimental value in good agreement with calculated one. This means that first, the values get from the model could be meaning-full despite the crude assumptions and, second, confirms the main origin of energy dissipation : adhesive mechanical instability [15, 23] as opposed to viscoelastic processes [28, 29].

4.2 single-wall CNT

4.2.1 Experimental results

Figure 10 presents data obtained from a single CNT directly grown on a Si tip. The three domains corresponding to the different regimes (from the right to the left : no interaction, intermittent contact and permanent contact) can be again distinguished unambiguously both in the frequency shift and interaction dissipated energy.

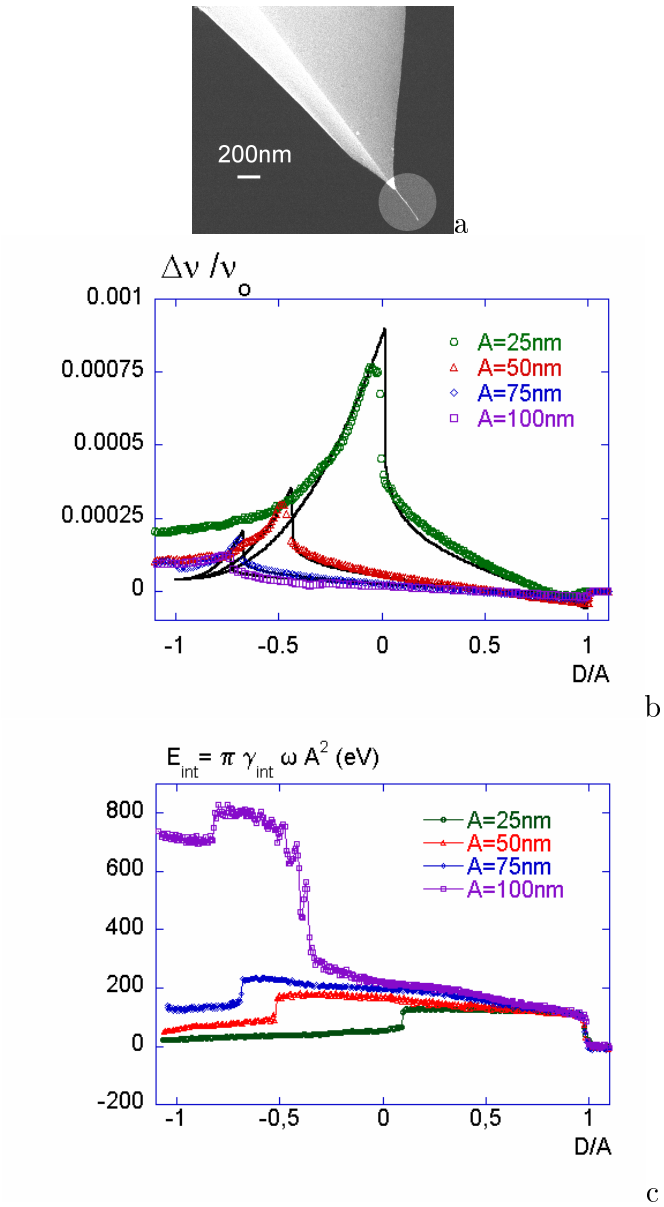

Figure 10: Data recorded with a single-wall CNT. Fig10.a : Scanning electron micrograph of the CNT long of about 500nm with a radius of 2nm. Fig. 10b: relative frequency shift variation with normalized distance for four amplitudes; experimental data in colored dots, fits with table 1 expressions in black lines. Fig. 10c : corresponding dissipated energy.

4.2.2 Frequency shifts

Here again the calculated values are in good agreement with the experimental frequency shifts (figure 10) using the observed pull off length $\Delta \approx 30\,nm$ and the parameters $\frac{k_r}{k_c} \approx 4.10^{-5}$ and $\frac{k_a}{k_c} \approx 0.002$. With the cantilever stiffness $k_c \approx 30 N.m^{-1}$, it gives $k_\mathrm{r} \approx 1.10^{-4}\,N.m^{-1}$ and $k_\mathrm{a} \approx 6.10^{-2}\,N.m^{-1}$. The bending stiffness is again of the same order than the calculated bending stiffness $k_\mathrm{b} = \pi E \frac{r^4}{L^3} \approx 4.10^{-4}\,N.m^{-1}$. The adhesive force is : $F_{adh} = k_{adh}\Delta \approx 1.8\,nN$, thus a smaller value than for the MWCNT. Whittaker et al [30] performed adhesion measurements of single-wall CNT embedded in silicon dioxide trenches, they obtained values around 10nN. This value is larger than the one obtained here, but the length of the CNT embedded in the structure could explain the difference.

Assuming again a nanotube gliding along the graphite surface, we evaluate a contact length of about $7\,nm$, a value slightly larger than the multi-wall CNT one.

4.2.3 Dissipation

The calculated value gives an amount of additional dissipated energy $E_{diss} = \frac{1}{2}k_{adh}\Delta^2 \approx 170\,eV$, thus one order of magnitude smaller than for the multi-wall CNT. The experimental dissipation energy remains roughly constant during the intermittent contact regime, except for the highest amplitude where probably a second nanotube is involved in the contact with the surface. The height of the plateau varies from 120 to 230 eV , thus the calculated value is close to the experimental ones.

4.3 Balancing the elastic and adhesive contributions

As seen in figure 8, the analytical expressions predicted a prevailing adhesive contribution for small amplitudes. Approach-retract curves have been performed with smaller oscillation amplitudes for the multi-wall CNT shown in figure 11a. The resulting frequency shifts are shown in figure 11b.

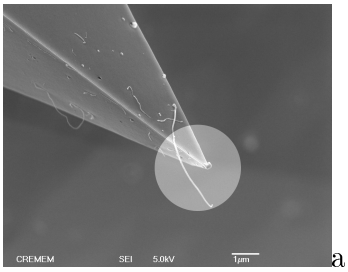

a

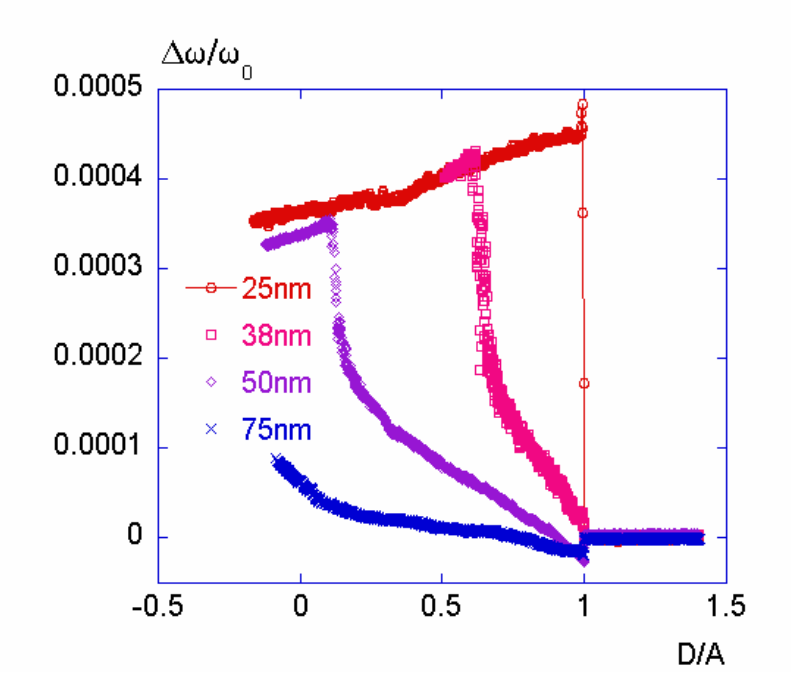

b

Figure 11: Data recorded on a MWCNT. Fig.9a : MEB image of the MWCNT of approximately 2 μm long and 50nm diameter. Fig.9b: Variation of the normalized experimental pulsation with normalized distance for four amplitudes.

There is a good agreement between the calculated curves 8 and experimental ones 11. At

the amplitude of $38\,nm$, the negative part of the frequency shift vanishes, the frequency shift becomes positive as soon as the CNT touches the surface. When the amplitude gets even lower, the intermittent domain disappears. As soon as the CNT touches the surface, it is unable to unstick. In other words, the elastic force is unable to overcome the adhesive force. As shown with these experimental data, it is easy to find the threshold amplitude below which the bending elasticity gives a negligible contribution, in turn has a weak effect, if any, on the contrast of an AFM image. As a consequence, it is of primary importance to determine the balance between the two forces in order to better understand the AFM images..

5 Conclusion

In this paper we have presented a comparative study of the mechanical properties of SWNT and MWNT fixed at an AFM tip apex. Since the beginning of the development of the CNT synthesis, CNT have been considered as excellent materials to use as a nanoprobe. Consequently, the obvious main goal of the present work is to improve a little more our basic understanding of the CNT behaviors at a tip apex. Beside a systematic experimental study of the CNT properties, a rather crude, but analytical, model was developed. The model includes two spring constants, one related to the elastic bending of the NT, the second to the pull off force required to unstick the NT. The calculated values are in excellent agreement with the experimental results recorded in approach curves done with multi and single-wall carbon nanotubes. As expected, a smaller equivalent stiffness is found for the single-wall as opposed to the multi-wall nanotube. The equivalent attractive stiffness and the distance necessary to unstick enable adhesion force evaluation with values comparable to other studies. Thus this model may be a way not only to understand AFM images but also to quantify different CNT mechanical behaviors.

This understanding and quantification of the CNT-probe properties should help to find good conditions to image complex sample. As the CNT behavior strongly depends on its boundary conditions on both the tip and surface, it could help to find a protocol to ensure its fixation to a support when the anchoring is not reached.

In spite of the excellent agreement between the theoretical description and the experimental values, a more exhaustive analysis must include several other parameters. In particular, the crude assumption used cannot allow to understand the increase of the dissipated energy during the intermittent contact. Further developments should include a tangential force component like friction, and a change of the contact area as a function of the vertical displacement. The influence of the angle between the surface and the nanotube probe is under study: nanotubes with a large angle as respect to the tip axis usually have a small repulsive stiffness value.

Acknowledgments

The authors gratefully acknowledge Cattien V. NGUYEN and Anne-Marie BONNOT for providing the multi-wall and single-wall carbon nanotubes respectively for this paper and Julien Buchoux for the welding of Figures 1 and 11 nanotubes. It is a pleasure to thank Elisabeth Sellier for some SEM micrographs. C'Nano Grand Sud Ouest and the Aquitaine Region are thankfully acknowledged for providing founds for this research.

References

[1] Iijima S; Brabec C; Maiti A; Bernholc J , *J.Chem.Phys.*, vol. 104, pp. 2089–2092, 1996.

[2] Collins Ph.G. and Avouris Ph., "Nanotubes for electronics," *Scientific American*, pp. 62–70, 2000.

[3] Cumings J., Collins P. and Zettl A., *Nature*, vol. 406, p. 586, 2000.

[4] Fennimore A.M.et al, *Nature*, vol. 424, pp. 408–410, 2003.

[5] Ke C., Espinosa H.D., *Appl. Phys. Lett.*, vol. 85, pp. 681–683, 2004.

[6] Lu JP, "Elastic properties of carbon nanotubes and nanoropes," *Phy.Rev. Lett.*, vol. 79, pp. 1297–1300, 1997.

[7] Zhang M , Fang S, Zakhidov A.A., Lee S.B., Aliev A. E., Williams C.D., Atkinson K.R., Baugghman R.H., "Strong, transparent, multifunctional, carbon nanotube sheets," *Science*, vol. 309, pp. 1215–1219, 2005.

[8] Treacy M. M., Ebbesen T. W. & Gibson J.M., "Exceptionally high young's modulus observed for individual carbon nanotubes," *Nature*, vol. 381, pp. 678–680, 1996.

[9] Wong EW; Sheehan PE; Lieber CM, "Nanobeam mechanics : elasticity, strength and toughness of nanorods and nanotubes," *Science*, vol. 277, pp. 1971–1975, 1997.

[10] Salvetat JP; Andrew G., Briggs D., Bonard J.M., Bacsa R.R., Kulik A.J., Stöckli T., Burnham N.A.,1 and Forró L. , "Elastic and shear moduli of single-walled carbon nanotube ropes," *Phys.Rev.Lett.*, vol. 82, pp. 944–947, 1999.

[11] Kis A, Csanyi G., Salvetat J.P., Lee T. N., Couteau E, Kulik A. J. , Benoit W., Brugger J. and Forro L., *Nature Materials*, vol. 3, p. 153, 2004.

[12] Stevens R; Nguyen C; Cassel A; Delzeit L; Meyyappan M; Han, "Improved fabrication approach for carbon nanotube probe devices," *J. Appl.Phys.Lett.*, vol. 77, pp. 3453–3455, 2000.

[13] Marty L; Bouchiat V; Naud C; Chaumont M; Fournier T; Bonnot AM , *Nano Lett.*, vol. 3, pp. 1115–1118, 2003.

[14] L.D. Landau and E.M. Lifshitz, *Theory of elasticity*, Pergamon Press , London, Ed., 1959.

[15] Dürig U., "Interaction sensing in dynamic force microscopy." *New J. Phys.*, vol. 2, pp. 5.1–5.12, 2000.

[16] Nony, L., Boisgard, R., Aimé, J.-P., "Nonlinear dynamical properties of an oscillating tip-cantilever system in the tapping mode." *J. Chem. Phys.*, vol. 111, no. 4, pp. 1615–1627, 1999.

[17] Goldstein, H., *Classical Mechanics.* Addison-Wesley, Reading, 1980.

[18] L. N. G. Couturier, R. Boisgard and J. P. Aimé, "Noncontact atomic force microscopy: Stability criterion and dynamical responses of the shift of frequency and damping signal," *REVIEW OF SCIENTIFIC INSTRUMENTS*, vol. 74, no. 5, pp. 2726–2734, 2003.

[19] Snow E. S. ,Campbell P. M. , and Novak J. P. , "Single-wall carbon nanotube atomic force microscope probes," *Appl. Phys. Lett.*, vol. 80, pp. 2002–2004, 2002.

[20] Solares S. D., Matsuda Y., and Goddard III W. A., "Influence of the carbon nanotube probe tilt angle on the effective stiffness and image quality in tapping mode atomic force microscopy." *J. Chem. Phys.B*, vol. 109, pp. 16 658–16 664, 2005.

[21] Kutana A.,Giapis K. P. ,Chen J. Y. , and Collier C. P. , "Amplitude response of single-wall carbon nanotube probes during tapping mode atomic force microscopy : modeling and experiment." *Nanoletters*, vol. 8, pp. 1669–1673, 2006.

[22] Maugis D., "Subcritical crack growth, surface energy, fracture toughness, stick-slip and embrittlement," *Mater. Sci.*, vol. 20, pp. 3041–3073, 1985.

[23] Dietzel D., Marsaudon S., Aimé J. P. , Nguyen C. V. and Couturier G., "Mechanical properties of a carbon nanotube fixed at a tip apex: A frequency-modulated atomic force microscopy study," *Physical Review B*, vol. 72, p. 035445, 2005.

[24] Dietzel D., Bernard C., Mariolle D., Iaia A., Bonnot A.M., Aimé J. P. , Marsaudon S., Bertin F. , and Chabli A., "Mechanical properties of carbon-nanotube tips and nanoneedles: A frequency modulation-atomic force microscope comparative study," *Journal of Scanning Microscopy*, vol. 1, pp. 45–50, 2006.

[25] Boisgard, R., Michel, D., Aimé, J.-P., "Hysteresis generated by attractive interaction: Oscillating behavior of a vibrating tip-microlever system near a surface." *Surf. Sci.*, vol. 401, pp. 199–205, 1998.

[26] Walkeajärvi T; Leivonen J; Ahlskog A , "Bending of multiwalled carbon nanotubes over gold lines," *J.of Appl.Sci.*, vol. 98, p. 104301, 2005.

[27] Israelachvili, J.N., *Intermolecular and Surface Forces.*, 2nd ed. Academic Press, New York, 1992.

[28] Boisgard R., AiméJ. P. , Couturier G., "Analysis of mechanisms inducing damping in dynamic force microscopy : Surface viscoelastic behavior and stochastic resonance process," *Applied Surface Science*, vol. 188, pp. 363–371, 2002.

[29] F. Dubourg, J. P. Aimé, S. Kopp-Marsaudon, R. Boisgard, Ph. Leclère, R. Lazzaroni, "Probing viscosity at the nanometer scale in a polymer melt with an oscillating tip." *Eur. Phys. J. E.*, vol. 6, pp. 49–55, 2001.

[30] Whittaker J D; Minot ED; Tanenbaum DM McEueun PL Davis RC, "Measurement of the adhesion force between carbon nanotubes and a silicon dioxide substrate." *Nano Lett.*, vol. 6, pp. 953–957, 2006.